Peter-Andreas von Wolffersdorff
Radu Schwab

Uelzen I Lock – Hypoplastic Finite-Element Analysis of Cyclic Loading

The Uelzen I Lock – hypoplastic finite-element analysis of cyclic loading. *The Uelzen I lock is a very suitable case to analyse the soil-structure interaction during cyclic loading because its plate-rib structure is very flexible, the amplitude of the load cycles during lock operation is high and an extensive geotechnical monitoring system was installed in 1992.*
A 3D finite element simulation was used to predict the long-term behaviour of the lock during cyclic loading. The main interest of the simulation was to choose an adequate constitutive law to simulate the quasi-static cyclic behaviour of the soil. The adopted hypoplastic constitutive law with intergranular strain is briefly described in the paper. The computed results are compared with the measurements. The results of elastic-perfect plastic Mohr-Coulomb and hypoplastic simulations without intergranular strain are presented for comparison. Some interesting aspects are evidenced, such as the 'stick-slip' reduction of the arching effect in the backfill due to cyclic loading.

Die Schleuse Uelzen I ist wegen ihrer flexiblen Tragstruktur, den großen Lastwechseln während des Schleusenbetriebes und der 1992 installierten, umfangreichen meßtechnischen Überwachung ein sehr gut geeignetes Anwendungsbeispiel, um das Interaktionsverhalten zwischen Bauwerk und Boden unter zyklischen Beanspruchungen zu untersuchen.
Es werden dreidimensionale Finite-Elemente-Berechnungen durchgeführt, um das Langzeit-Verhalten der Schleuse bei zyklischen Beanspruchungen zu prognostizieren. Entscheidend dafür ist, daß das Stoffmodell für den Boden auch das quasi statische zyklische Verhalten realitätsnah erfaßt. Das verwendete hypoplastische Stoffmodell mit intergranularer Dehnung wird kurz beschrieben. Die Ergebnisse der numerischen Berechnungen werden mit gemessenen Setzungen der Schleuse verglichen. Es werden zum Vergleich die Ergebnisse von hypoplastischen Berechnungen ohne intergranulare Dehnung und von elastisch-idealplastischen Berechnung mit dem Mohr-Coulombschen-Modell vorgestellt. Siloeffekte im Hinterfüllungsbereich zwischen den Rippen der Schleuse verringern sich infolge der zyklischen Beanspruchungen in Verbindung mit „stick-slip"-Verhalten

1 Introduction

The Uelzen I lock, which began operating in 1976, is one of the highest locks in Germany, with a rise of 23 m. The lock is around 185 m long and 12 m wide. Owing to the increase in traffic on the Elbe Lateral Canal between the port of Hamburg and the network of canals linking Hanover and Berlin, it was decided to build a second lock directly adjacent to the existing one (see figure 1)

The Uelzen I lock was constructed with water-saving basins so that less water is moved in the canal during lockage operations. It comprises the lock structure, the water-saving basins and a control house located in between. The lock chamber was designed as a very slender reinforced steel plate-rib structure. The chamber walls are 75 cm thick and are stiffened by 8 m wide cantilevered 1.5 m thick ribs.

When it was built, the lock was referred to as a "breathing" lock as it had been designed to allow a high level of deformation during lockage operations. However, damage to the concrete structure occurred unexpectedly and was found be the result of, amongst other things, insufficient consideration having been given to the soil-structure interaction during cyclic loading due to operation of the lock. The lock has since been repaired several times. The existing lock has been continuously monitored ever since damage occurred, with special attention being paid to its deformations and movements.

The in-situ soil exhibits the effects of glaciation and comprises three main layers (see figure 2). An approximately 15 m thick layer of boulder clay with low permeability lies beneath a layer of upper sand which is several metres thick. Lower sand, which was highly overconsolidated during glaciations, is to be found beneath the boulder clay.

Figure 2 also shows the profile of the earlier sloped pit excavated to allow construction of the Uelzen I lock. The pit was backfilled with sand with properties corresponding largely to those of the upper sand.

The current project originated as a result of the extensive deformation measurements being conducted at the Uelzen I lock. Its aim is to investigate the deformation behaviour of the soil and the structure under cyclic loading by performing a 3D finite element simulation based on a novel hypoplastic constitutive law. The law enables the mechanical behaviour of cohesionless soils under cyclic loading to be described by means of the intergranular strain, which is an internal state variable.

2 Hypoplastic constitutive law

2.1 Preliminary remarks

The hypoplasticity theory was developed at the Institute of Soil Mechanics and Rock Mechanics of the University of Karlsruhe over a 20-year period. The fundamentals of the theory were established by *Kolymbas* [5]. The version of the constitutive law presented in this article is the result of many years of research into the law by a team of specialists.

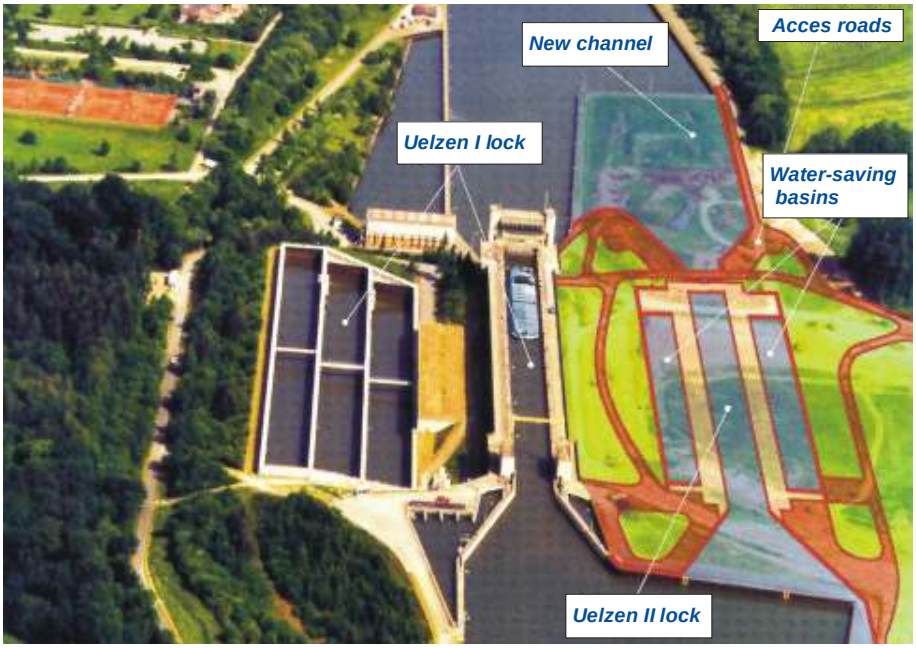

Fig. 1: Aerial view of the existing Uelzen I lock and the new Uelzen II lock (under construction)

The aim of this article is to demonstrate how hypoplasticity can be applied. A brief summary of the mathematical formulation of the hypoplastic constitutive law is given in Annexes A and B. The theoretical basis and mathematical formulation of the hypoplastic constitutive law are described in detail in [1], [9], [11], [12], [13]. The determination of the material parameters, which in contrast to the parameters of many other material constitutive laws in soil mechanics are physically well founded, is described in detail in [2], [3], [6].

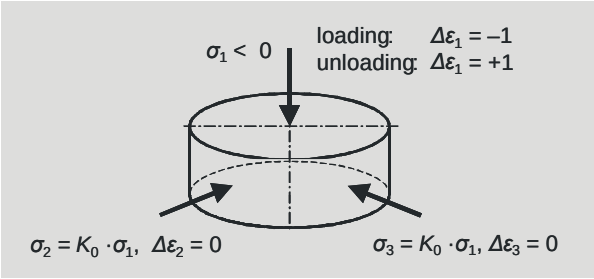

Fig. 3: Boundary and loading conditions in the oedometer test

The principal mode of operation of the original version of the hypoplastic constitutive law under uniaxial deformation and of the extended version with intergranular strain is explained in the following sections.

The simple case referred to here is illustrated in figure 3, taking the conventional edometer test with a predefined increase in deformation, $\Delta\varepsilon_1 = \pm 1$, as an example. The equation $\sigma_2 = \sigma_3 = K_0 \cdot \sigma_1$ applies to the main stress components. The ratio of radial stress to vertical stress is the coefficient of the at rest lateral earth pressure, K_0. The rules for negative and positive signs in mechanics apply here (tension: +, pressure: –).

2.2 Version without intergranular strain

A distinction between state variables and material parameters is already consistently drawn in the original hypoplastic constitutive law (without intergranular

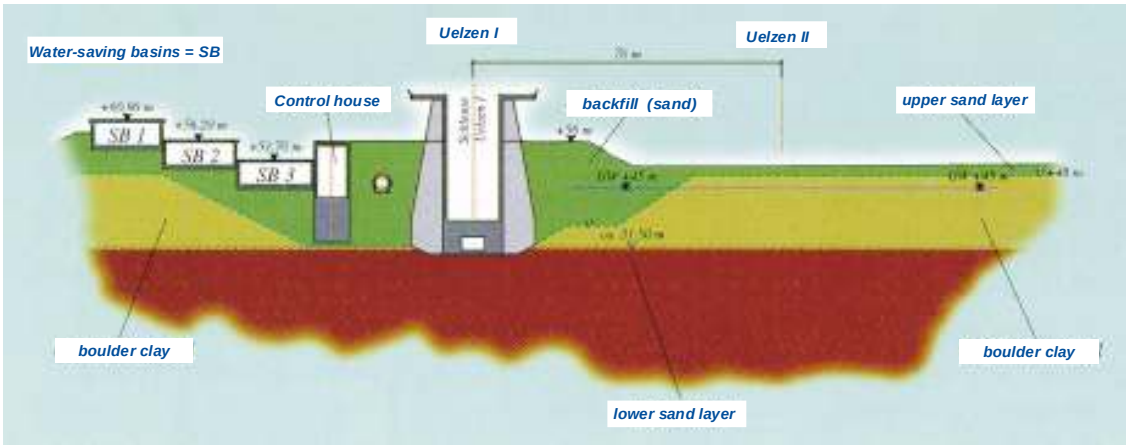

Fig. 2: Uelzen I lock – cross-section of the structure and soil profile

strain). The state variables are the actual stress, σ, and the actual void ratio, e. The stress response, Δσ, is obtained as follows according to the hypoplasticity theory:

$$\Delta\sigma = L(\sigma, e) \cdot \Delta\varepsilon + N(\sigma, e) \cdot \|\Delta\varepsilon\| . \quad (1)$$

The stress response comprises the component $L(\sigma, e) \cdot \Delta\varepsilon$, which is linear in Δε, and the component $N(\sigma, e) \cdot \|\Delta\varepsilon\|$, which is non-linear in Δε, where $\|\Delta\varepsilon\|$ is the Euclidean standard for Δε. The following applies in the principal component system:

$$\|\Delta\varepsilon\| = \sqrt{\Delta\varepsilon_1^{\,2} + \Delta\varepsilon_2^{\,2} + \Delta\varepsilon_3^{\,2}} . \quad (2)$$

In the above case of 1D compression, in which $\Delta\varepsilon_2 = \Delta\varepsilon_3 = 0$, $\|\Delta\varepsilon\|$ is simplified to $|\Delta\varepsilon_1| = 1$. The specifications for $L(\sigma, e)$ and $N(\sigma, e)$ for general 3D states and for the boundary conditions of the oedometer test shown in figure 3 are given in Annex A and in Annex C respectively.

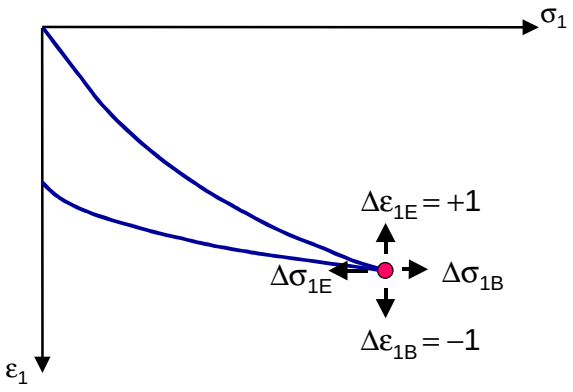

Fig. 4: Hypoplastic model without intergranular strain – oedometric loading and unloading

Figure 4 shows that the hypoplastic model results in different stress responses, $\Delta\sigma_{1B}$ and $\Delta\sigma_{1E}$, for oedometric loading and unloading, i.e. $\Delta\varepsilon_{1B} = -1$ and $\Delta\varepsilon_{1E} = +1$ respectively. Under the boundary conditions of the edometer test eq. (1) is simplified as follows:

On loading: $\Delta\sigma_{1B} = -L_{11} + N_1$

On unloading: $\Delta\sigma_{1E} = L_{11} + N_1$

It is evident that $\|\Delta\sigma_{1E}\|$ is grater than $\|\Delta\sigma_{1B}\|$, i.e. the incremental stiffness on unloading is greater than that on loading. According to the hypoplasticity theory, different material behaviours on loading and unloading can be defined very simply without the need to resort to the mathematical instrument of the classical plasticity theory which comprises the yield surface, flow rule and consistency condition.

However, the disadvantage of the original hypoplastic theory is that the behaviour of soils during cyclic loading (i.e. repeated loading and unloading) cannot be modelled realistically in spite of the second state variable, e, being taken into account and an effect known as ratcheting occurs (see figure 7a).

2.3 Version with intergranular strain

Niemunis and *Herle* [9] expanded the original hypoplastic law for cyclic loading by introducing an additional state variable, which is the intergranular strain, S. The following, more general relationship applies to the stress response, Δσ:

$$\Delta\sigma = F(\sigma, e, S, \Delta\varepsilon) . \quad (3)$$

The mode of operation of the intergranular strain, S, is shown for 1D compression in a simplified way in figure 5. The complete mathematical formulation for general 3D states is given in Annex B.

As shown in figure 5, S increases under monotonic loading up to its maximum value, R, and remains constant under further deformation. The intergranular strain, S, and the deformation, $\Delta\varepsilon_1$, act in the same direction. "Pure" hypoplastic behaviour exists in this state.

During the subsequent reversal of deformation with a 180° change in direction the intergranular strain, S, initially corresponds to R and maintains its initial direction. As the deformation reversal progresses, the intergranular strain, S, decreases until $S = 0$ and then increases again in the opposite direction until the maximum value, R, is reached.

Owing to the effect of S, the incremental stiffness, dE, is considerably greater after a deformation reversal of 180° than if the deformation had not been reversed (see figure 5). The incremental stiffness decreases in line with the increase in deformation and again reaches the initial hypoplastic stiffness at $\varepsilon_1 = \varepsilon_{SOM}$ (SOM – **s**wept **o**ut of **m**emory).

Changing the direction of deformation by 90° reduces the effect of S, i.e. the incremental stiffness is lower than for a deformation reversal of 180°. 90° changes in the direction of the deformations are ruled out in the case of 1D compression, e.g. in the edometer test, but occur in multi-dimensional tests, such as the triaxial or biaxial tests.

It can be seen in figure 6 that the hypoplastic model with intergranular strain provides a more pronounced stress response, $\Delta\sigma_{1E}$, at reversal point A on oedometric unloading, $\Delta\varepsilon_{1E} = +1$, than the "pure" hypoplastic model and that the initial hypoplastic incremental stiffness is not achieved again until the SOM point B is reached.

The following three different stress responses can be defined for oedometric loading and unloading:

On loading: $\Delta\sigma_{1B} = -L_{11} + N_1$

On unloading, at reversal point A: $\Delta\sigma_{1E} = m_R \cdot L_{11}$

On unloading, at SOM point B: $\Delta\sigma_{1E} = L_{11} + N_1$

The effect of intergranular strain results, at reversal point A, in hypoelastic behaviour that is stiffer than the initial hypoplastic behaviour on unloading and is described by

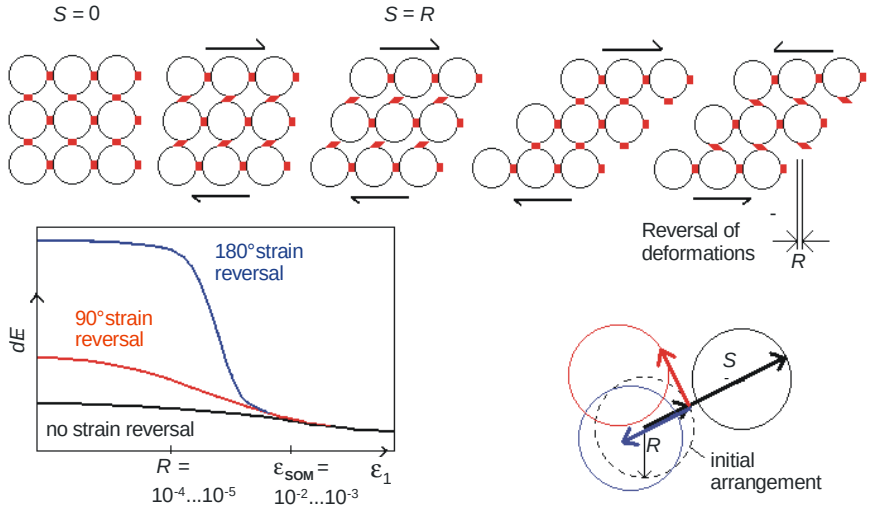

Fig. 5: Mode of operation of the intergranular strain – 1D shearing (according to [6])

the increase factor, m_R. Accordingly, $\|\Delta\sigma_{1EA}\| > \|\Delta\sigma_{1EB}\| > \|\Delta\sigma_{1B}\|$, i.e. the incremental hypoelastic stiffness on unloading at reversal point A is greater than the incremental stiffness at SOM point B during oedometric unloading. The incremental stiffness on loading is lower than both incremental stiffnesses on unloading.

The higher incremental hypoelastic stiffness also applies on renewed oedometric loading, so that hysteresis loops develop in the cycles and ratcheting does not occur. Figure 7b shows that the hypoplastic model with intergranular strain is able to realistically describe the material behaviour of cohesionless soils under cyclic loading, as demonstrated by oedometric loading, unloading and renewed loading.

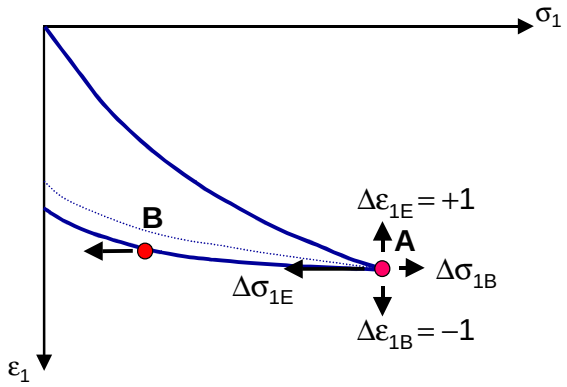

Fig. 6: Hypoplastic model with intergranular strain – oedometric loading and unloading

2.4 Material parameters

The basic hypoplastic model requires a total of eight material parameters. Five additional material parameters are required for the extension with intergranular strain. The integration of the material parameters into the mathematical formulation of the model is shown in Annexes A and B.

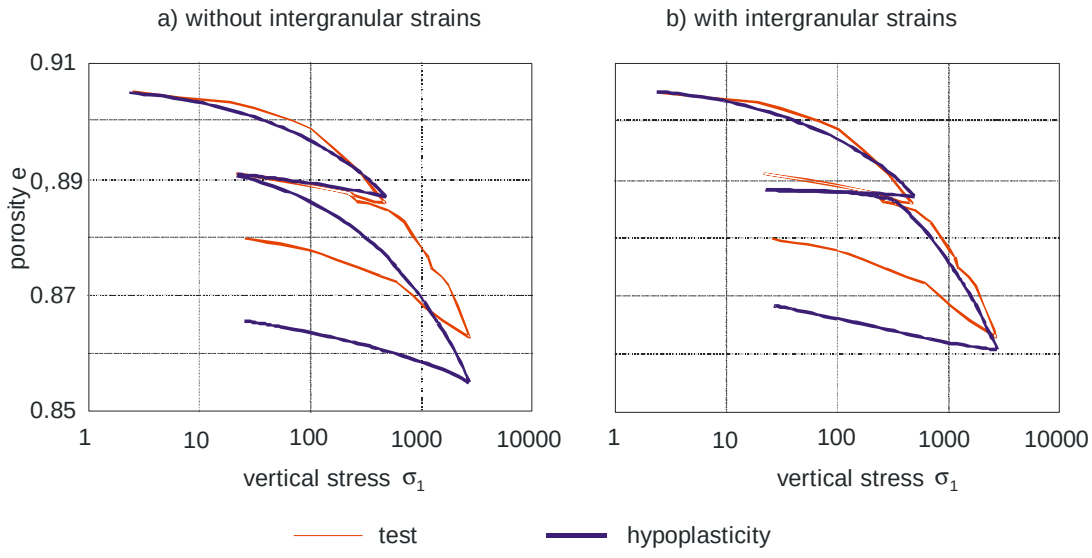

Fig. 7: Results of an oedometer test and hypoplastic back-calculation (according to [7])

The hypoplastic finite-element simulations for the Uelzen I lock were performed with the data sets given in table 1.

Table 1: Material parameters of the hypoplastic soil model (lower sand, boulder clay and backfill)

Material parameters of the basic hypoplastic model		Lower sand	Boulder clay	Backfill
granular stiffness	h_s	8500 MPa	210 MPa	6000 MPa
Critical friction angle	φ_c	35°	30°	30°
Critical void ratio	e_{c0}	1.01	0.91	1.01
Void ratio at maximum compaction	e_{d0}	0.613	0.523	0.613
Compression exponent	n	0.467	0.31	0.467
Pycnotropy exponent	α	0.1175	0.19	0.1175
Pycnotropy exponent	β	1.0	1.0	1.0
Void ratio at minimum compactionl	e_{i0}	1.163	1.09	1.163
Material parameters for the extension with intergranular strain				
Maximum intergranular strain	R	0.0001	0.0001	0.0001
Increase factor at 180° change in direction	m_R	5	5	5
Increase factor at 90° change in direction	m_T	2	2	2
Exponent	β_r	0.5	0.5	0.5
Exponent	χ	6	6	6

The material parameters for the basic hypoplastic model can be estimated with sufficient accuracy from simple classification tests or from the granulometric properties. The determination of the parameters is described in detail in [2], [3]. The determination of the five additional material parameters needed for the extension with intergranular strain is explained in [9]. The model parameters for lower sand were determined at the Institute of Soil Mechanics and Rock Mechanics of the University of Karlsruhe.

3 Calculations for the Uelzen I lock

3.1 General

The behaviour of the Uelzen I lock is influenced to a great extent by the interaction between the structure and the surrounding soil (backfill, lower sand strata). As a result, arching effects arise in the lateral backfill between the ribs of the structure.

Cyclic loading due to operation of the lock is responsible for a large proportion of the long-term settlement of the structure. The lower sand stratum is a major influence on such settlements.

The finite element simulations were performed with the ABAQUS software. The hypoplastic model was implemented in the form of a USER routine, the basic structure of which is shown in [8].

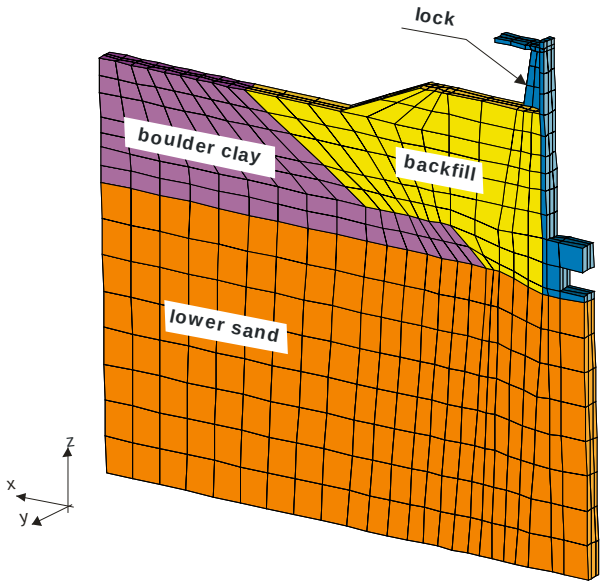

Fig. 8: 3-D finite element model

3.2 3D finite element model

When drawing up the 3D finite element model shown in figure 8 advantage was taken of the symmetry of the structure and the former construction pit so that only one half of the lock chamber with the corresponding soil strata – i.e. backfill, boulder clay, lower sand – was modelled. The model has a thickness of 2.5 m in direction (2) and is limited to half the thickness of a rib with half the distance between two ribs.

The following four options for soil models were simulated:

- Option A: Hypoplastic model with intergranular strain for lower sand, boulder clay and backfill.
- Option B: Hypoplastic model with intergranular strain for lower sand and boulder clay, elastic rigid-plastic *Mohr-Coulomb* soil model for backfill.
- Option C: Hypoplastic model without intergranular strain for lower sand, elastic rigid-plastic *Mohr-Coulomb* soil model for boulder clay and backfill.
- Option D: Elastic rigid-plastic *Mohr-Coulomb* soil model for lower sand, boulder clay and backfill.

Table 2: Material parameters of the elastic rigid-plastic Mohr-Coulomb soil model and unit weight of soil

Material parameters for the *Mohr-Coulomb* soil model		Lower sand	Boulder clay	Backfill
Modulus of elasticity	E	600 MPa	50 MPa	20-40 MPa
Poisson's ratio	ν	0.25	0.32	0.30
Friction angle	φ	42.5°	30°	30-35°
Cohesion	c	0	10	0
Dilatancy angle	ψ	12°	7°	0-5°
Other soil parameters		Lower sand	Boulder clay	Backfill
Wet unit weight	γ	21 kN/m³	21.5 kN/m³	20 kN/m³
Unit weight at buoyancy	γ'	11 kN/m³	11.5 kN/m³	10 kN/m³

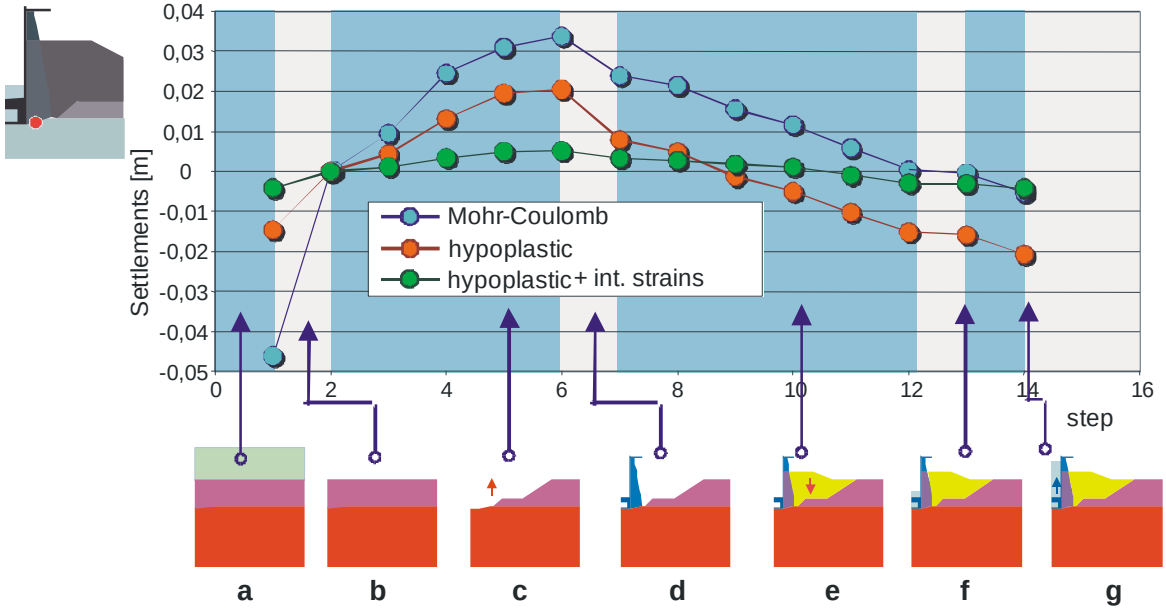

Fig. 9: Loading history and displacements of a point beneath the lock foundation

The data sets for the finite element simulations in which the Mohr-Coulomb soil model was used are given in table 2.

The concrete used in the lock was assumed to be linear-elastic with elasticity parameters as specified in the German standard DIN 1045.

3.3 Initial state

Modelling the initial state has a particular significance when the hypoplastic constitutive law is applied as the three state variables σ, e and S required for that purpose must be specified in the finite element model. The state variables are permitted to deviate from the equilibrium condition to only a very small degree, i.e. they must be compatible with the constitutive law.

Prior to the first phase of the simulation, referred to as "initial loading due to glaciation" (see figure 9 and table 3), the vertical stress, $T_{v0} = -\gamma \cdot h$, and the horizontal stresses, $T_{h0} = K_0 \cdot T_{v0}$, were defined as initial stresses. The coefficient of the at rest value of earth pressure, K_0, was determined approximately by means of *Jaky's* equation. In the initial state the pressure level, $\mathrm{tr}\mathbf{T}_0$, is as follows:

$$\mathrm{tr}\mathbf{T}_0 = -(1 + 2 \cdot K_0) \cdot \gamma \cdot h \qquad (4)$$

The compression law described in Annex A (A.8) is applied as follows to determine the initial void ratios, e_0:

$$e_0 = e_{00} \cdot \exp\left[-\left(\frac{-\mathrm{tr}\mathbf{T}}{h_s}\right)^n\right] \qquad (5)$$

In eq. (5), e_{00} is an estimated void ratio for the three densely compacted soils. It was assumed to be around 20 % greater than the void ratio at the maximum shear compaction, e_{d0} ($e_{00} \approx 1.2 \cdot e_{d0}$).

In addition, it was also assumed that, in the initial state, there are only fully mobilised intergranular strains in the direction of the earth's acceleration, i.e. $S_{v0} = R$ and $S_{h0} = 0$.

The initial void ratios, $e_{0,}$ determined in accordance with (4) are inconsistent with the hypoplastic constitutive law as the predefined stresses, $T_{h0} = K_0 \cdot T_{v0}$, are not fully compatible with it. This approximation has been shown to be sufficiently accurate as regards convergence in the first steps of the finite element simulation.

3.4 Loading history

A large number of calculation steps had to be generated within the 3D model (figure 9 and table 3) as the soil behaviour modelled with hypoplasticity depends on the loading history. The simulation was highly complex and time-consuming which was due in particular to the cyclic loading (20 cycles from calculation steps f → g → f).

Table 3: Main steps of the simulation

Step	Description
a	Initial loading due to glaciations
b	Initial condition (free field)
c	Excavation for lock construction
d	Lock construction
e	Backfilling (5 calculation steps)
f	Tailwater in lock
g	Headwater in lock
	Lockage operations (20 cycles f → g → f)

The vertical displacements of a point beneath the lock foundation are shown in figure 9 in addition to the calculation steps a to g. Comparative simulations have been conducted to assess the influence of the constitutive law, with the lower sand stratum being modelled in the following three ways: the elastic rigid-plastic *Mohr-Coulomb* soil model, the hypoplastic model without

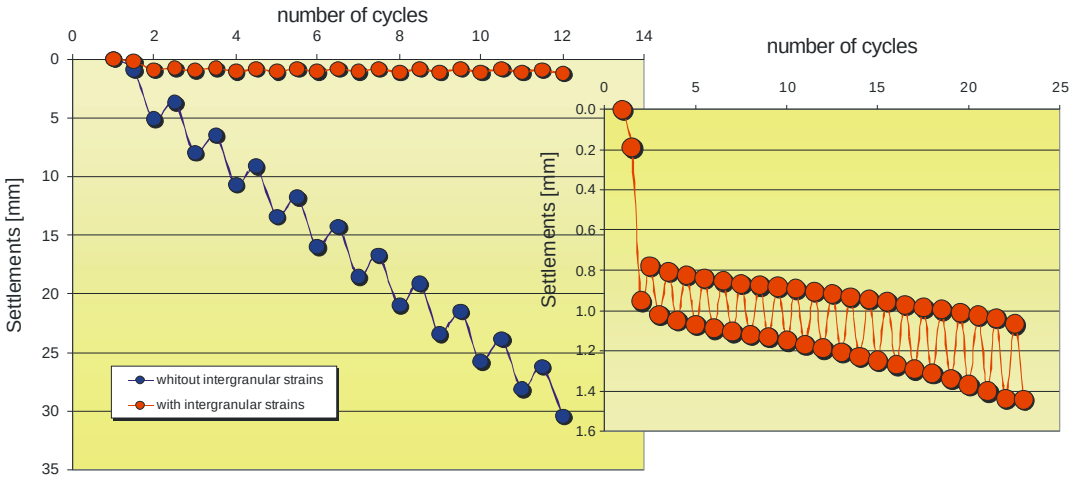

Fig. 10: Settlements of the Uelzen I lock due to cyclic loading

intergranular strain and the hypoplastic model with intergranular strain. As shown in figure 9, the hypoplastic simulation with intergranular strain produces the lowest degree of heave and settlement during the entire simulation procedure. Based on previous experience with the deformation behaviour of the Uelzen I lock, which was supported predominantly by measurements, it is these results that are considered the most realistic.

3.5 Cyclic behaviour

The lock was subjected to cyclic loading by lockage operations for around 20 years. The resultant cyclic deformations are partly reversible, but a significant proportion of those deformations has accumulated. Geodetic measurements at the Uelzen I lock have revealed an annual settlement of around 1 cm (see figure 15). The hypoplastic model was used to describe this effect.

The settlements calculated for a point beneath the lock foundation are shown in figure 10. As in the oedometer test, pronounced ratcheting occurs in the hypoplastic model without intergranular strain so that the settlements that occur are far too high. The settlements calculated using the hypoplastic model with intergranular strain show that ratcheting is avoided in part by local hypoelastic behaviour and the settlements increase to a much smaller degree.

As the deformation and settlement measurements conducted at the Uelzen I lock did not begin directly after completion of the lock, it is not possible to make a direct comparison of the results of the simulation and the results of the measurements (see figure 15). The large number of load cycles (several hundreds or thousands) that had taken place prior to the first measurements would first have to be calculated in order to do so. The effort required for a finite element simulation with so many load cycles is unrealistically high.

3.6 Arching effects

The distance between the ribs is only 3.5 m. Consequently, the lateral deformations of the backfill between the ribs are subject to kinematic constraints, giving rise to an arching effect. This effect is illustrated in figure 11 for the period prior to commencement of operation of the lock (step e of the simulation) and arises when the soil model option B is applied. The backfill is supported by the lock walls. This gives rise to shear stresses in the

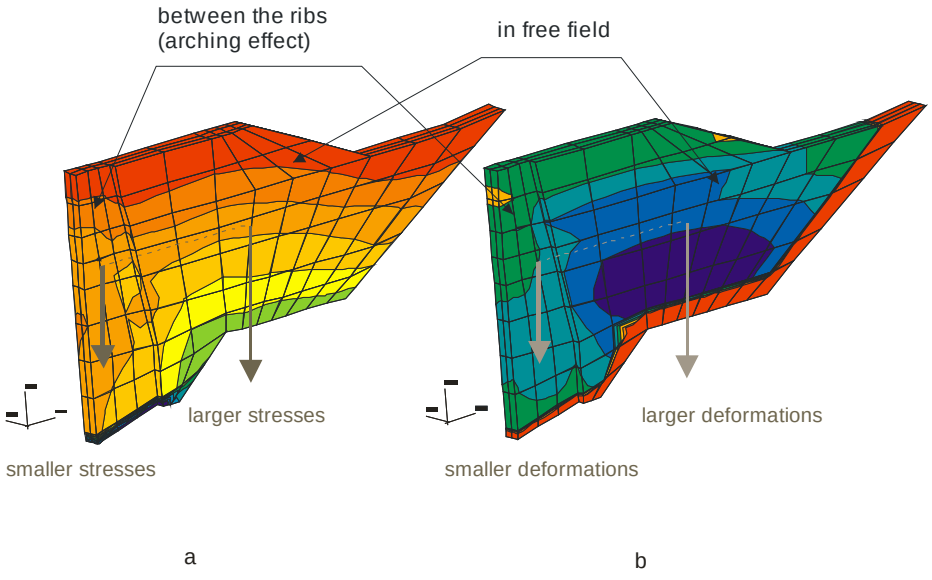

Fig. 11: Arching effects in the backfill: a) vertical stress distribution, b) distribution of vertical displacements

contact surfaces and the backfill deforms less than it would if it were unsupported (see figure 11b). The vertical normal stresses are consequently also lower than the own weight of the backfill (see figure 11a).

The simulation of the cyclic loading has revealed an interesting phenomenon. The arching effect in the backfill decreases to an ever greater extent under cyclic loading. This reduction occurs at the same time as failure occurs along the wall-soil boundary, giving rise to stick-slip behaviour (see figure 12).

In accordance with soil model option B, the slip at the wall first occurs after six cycles. For soil model option A the simulation was stopped after seven cycles without any stick-slip occurring. The numerical problems which led to the simulation being stopped occur in the interface elements and it has not yet been possible to resolve them.

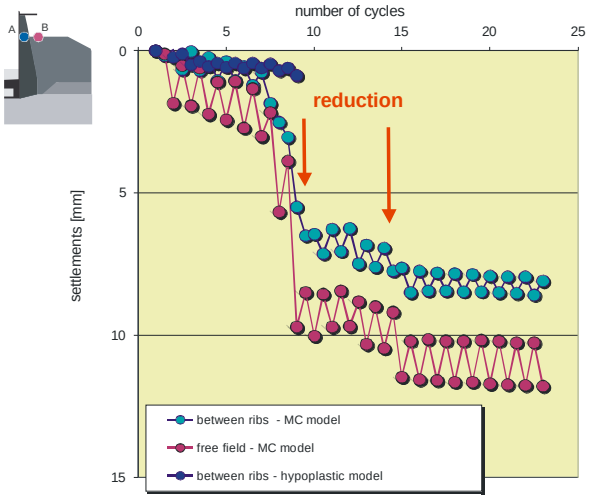

Fig. 12: Reduction of the arching in the backfill due to cyclic loading

Based on the current results of the simulations and measurements, it is not possible to assess whether the stick-slip behaviour established in the numerical simulations is realistic or whether it is a phenomenon caused by the interface elements used.

4 Measurements

An extensive monitoring system has been installed (figure 13) as the construction of the new Uelzen II lock in the immediate vicinity of the present lock affects the existing structure. The entire lock system, comprising the existing lock, the construction pit for the new lock/new lock structure and the surrounding soil, was modelled in a finite element model accompanying the construction work to provide a prediction of the deformations. The finite element model used acted as a tool with which the results of the measurements could be assessed [10].

The results of the extensometer measurements shown in figure 14 reveal three types of deformation:

– deformations caused by changes in temperature, shown by a sine curve over a period of one year,

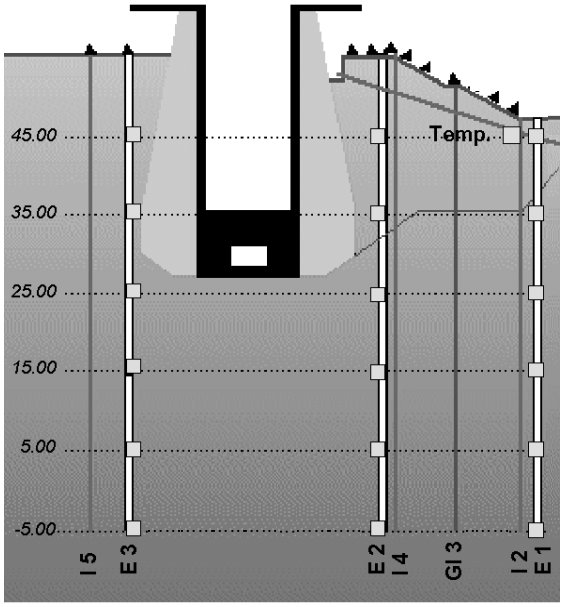

Fig. 13: Survey cross-section 1 (E extensometer, I inclinometer, GI chain inclinometer, Temp. temperature sensor)

– cyclic deformations caused by operation of the lock,

– accumulating residual deformations.

The magnitude of the measured deformations corresponds to the computed values. It is currently only possible to make a provisional comparison between the results of the measurements and those of the finite element simulations as construction of the new lock structure has not actually commenced as yet.

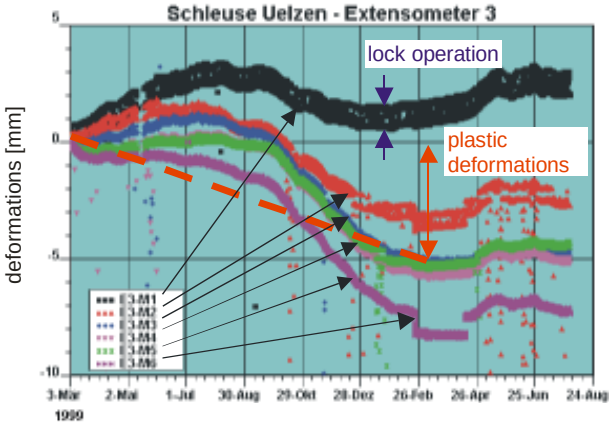

Fig. 14: Results of extensometer measurements

Figure 15 shows the results of the measurements of settlements at the Uelzen I lock as a function of the number of cycles during its operation (green dots). In order to be able to compare those results with the computed settlements (red dots) the results of the measurements were extrapolated onto the area with low numbers of cycles. As indicated in figure 15, the settlements of the Uelzen I lock computed on the basis of the hypoplastic constitutive law with intergranular strain are realistic.

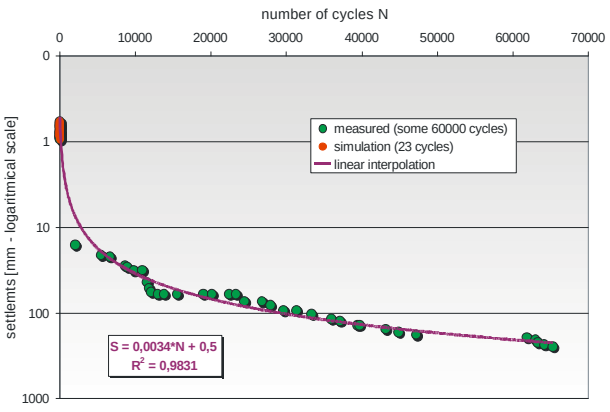

Fig. 15: Measured vs. computed settlements

5 Conclusions

The application of the hypoplastic constitutive law with intergranular strain permits realistic modelling of the soil-structure interaction under static and cyclic loading. As each individual load cycle is calculated in this method, the results provide a correct picture of the distributions of the stresses and deformations. Such analyses are limited to a small number of loading cycles as they are highly complex and time-consuming.

If a large number of cycles are to be modelled, it can be useful to apply a method in which the number of cycles is regarded as a pseudo-time variable and the cyclic behaviour is simulated by a model with pseudo-creep.

This article was written as part of the collaboration between the Federal Waterways Engineering and Research Institute, Karlsruhe, and the Institute of Soil Mechanics and Rock Mechanics of the University of Karlsruhe. The authors wish to thank G. Gudehus, I. Herle, G. Huber, C. Karcher, P. Kudella, P.-M. Mayer, A. Niemunis and K. Nübel in particular for their support and their many valuable comments.

Annex A – Hypoplastic model without intergranular strain – 3D-formulation

The following notation is used in this brief summary of the hypoplastic model: bold symbols for second-order tensors (e.g. **D**, **T**, **N, 1**), calligraphic symbols for fourth-order tensors (e.g. $\mathcal{L}$, $\mathcal{M}$, $\mathcal{I}$).

Tensorial multiplications or operations are written as follows: $\mathcal{L}:\mathbf{D} = L_{ijkl}D_{kl}$, $\mathbf{T}^2 = T_{ij}T_{kl}$, $\mathrm{tr}\mathbf{T} = T_{ij}$, $\mathrm{tr}(\mathbf{T}^2) = T_{ij}T_{ij}$, $\mathrm{tr}(\mathbf{T}^3) = T_{ij}T_{jk}T_{kl}$. The Euclidean standard for tensor **D** is $\|\mathbf{D}\| = \sqrt{D_{ij}D_{ij}}$. The second- and fourth- order unit tensors are defined as follows: $\mathbf{1} = \delta_{ij}$ and $\mathcal{I} = \delta_{ik}\delta_{jl}$, where $\delta_{ij} = \{1 \text{ for } i = j,\ 0 \text{ for } i \neq j\}$ is the *Kronecker* symbol.

The hypoplastic model can be represented by a single tensorial equation. According to [8] the following constitutive equation applies to the class of hypoplastic models:

$$\overset{\circ}{\mathbf{T}} = \mathcal{L}(\mathbf{T}, e):\mathbf{D} + \mathbf{N}(\mathbf{T}, e)\|\mathbf{D}\| \qquad (A.1)$$

i.e. the objective stress rate, $\overset{\circ}{\mathbf{T}}$ (*Jaumann* stress rate), is a function of the actual grain skeleton stress, **T** (*Cauchy* stress sensor), the rate of deformation, **D** (rate of deformation tensor), and the void ratio, e. As the model also includes the state variable e in addition to the actual grain skeleton stress, **T**, a second equation is required to derive the value of e by analogy to eq. A.1. It applies if the volume of the grains is constant:

$$\dot{e} = (1+e)\cdot \mathrm{tr}\mathbf{D} \qquad (A.2)$$

where $\dot{e}$ is the change in the void ratio and $\mathrm{tr}\mathbf{D}$ is the change in volume.

In eq. A.1 the operator $\mathcal{L}:\mathbf{D}$ is linear in **D** and the expression $\mathbf{N}\|\mathbf{D}\|$ is non-linear in **D**. The hypoplastic model is therefore non-linear in **D**.

According to the proposal put forward by *von Wolffersdorff* [11, 12], who developed the mathematical formulations for the model on the basis of *Matsuoka-Nakai*'s limit condition for critical states, the tensor functions $\mathcal{L}$ and **N** can be represented as follows:

$$\mathcal{L} = f_s \cdot \frac{1}{\mathrm{tr}(\hat{\mathbf{T}}^2)} \cdot \left(F^2 \mathcal{I} + a^2 \hat{\mathbf{T}}^2\right) \qquad (A.3)$$

$$\mathbf{N} = f_s \cdot f_d \cdot \frac{a \cdot F}{\mathrm{tr}(\hat{\mathbf{T}}^2)} \cdot \left(\hat{\mathbf{T}} + \hat{\mathbf{T}}^*\right) \qquad (A.4)$$

with the pressure level-related stress tensor, $\hat{\mathbf{T}} = \mathbf{T}/\mathrm{tr}\mathbf{T}$, and its deviator, $\hat{\mathbf{T}}^* = \hat{\mathbf{T}} - \frac{1}{3}\mathbf{1}$. The scalar stress function, F, is obtained from *Matsuoka-Nakai*'s limit condition as follows:

$$F = \sqrt{\frac{1}{8}\tan^2\psi + \frac{2-\tan^2\psi}{2+\sqrt{2}\tan\psi\cos 3\vartheta}} - \frac{1}{2\sqrt{2}}\tan\psi \qquad (A.5)$$

with $\tan\psi = \sqrt{3}\|\hat{\mathbf{T}}^*\|$ and $\cos 3\vartheta = -\sqrt{6}\,\frac{\mathrm{tr}\left(\hat{\mathbf{T}}^3\right)}{\left[\mathrm{tr}\left(\hat{\mathbf{T}}^2\right)\right]^{\frac{3}{2}}}$.

The two factors f_d and f_s describe the pressure and density dependency of the model. They are defined as follows:

$$f_d = \left(\frac{e - e_d}{e_c - e_d}\right)^{\alpha} \qquad (A.6)$$

$$f_s = \frac{h_s}{n}\cdot\left(\frac{e_i}{e}\right)^{\beta}\cdot\frac{1+e_i}{e_i}\cdot\left(\frac{-\mathrm{tr}\mathbf{T}}{h_s}\right)^{1-n} \mathrm{x}$$
$$\mathrm{x}\left[3 + a^2 - a\cdot\sqrt{3}\cdot\left(\frac{e_{i0} - e_{d0}}{e_{c0} - e_{d0}}\right)^{\alpha}\right]^{-1} \qquad (A.7)$$

e_c, e_d and e_i are characteristic void ratios and are dependent on the following compression law [1]:

$$\frac{e_c}{e_{c0}} = \frac{e_d}{e_{d0}} = \frac{e_i}{e_{i0}} = \exp\left[-\left(\frac{-\mathrm{tr}\mathbf{T}}{h_s}\right)^n\right] \qquad (A.8)$$

Apart from the auxiliary parameter, a, all variables and functions of the model have been defined. The parameter a is obtained from a simple relationship containing the critical angle of shearing resistance, φ_c:

$$a = \frac{\sqrt{3}\cdot(3-\sin\varphi_c)}{2\cdot\sqrt{2}\cdot\sin\varphi_c} \qquad (A.9)$$

The hypoplastic model includes a total of eight material parameters. The four basic parameters are as follows:

- Granular stiffness h_s [MPa],
- Critical friction angle φ_c [°],
- Critical void ratio e_{c0} [-] at $\mathrm{tr}\mathbf{T} = 0$,
- Void ratio at maximum compaction e_{d0} [-] at $\mathrm{tr}\mathbf{T} = 0$.

The additional material parameters are as follows:

- Compression exponent n [-],
- Pycnotropy exponent α [-],
- Pycnotropy exponent β [-],
- Void ratio at minimum compaction e_{i0} [-] at $\mathrm{tr}\mathbf{T} = 0$.

Annex B – Hypoplastic model with intergranular strain – 3D-formulation

In addition to the information given in Annex A the following notation is used for tensorial multiplications and operations in conjunction with the tensor for intergranular strain, $\mathbf{S}$: $\mathcal{L} : \hat{\mathbf{S}}^2 = L_{ijkl}\hat{S}_{kl}\hat{S}_{mn}$, $\hat{\mathbf{S}}^2 = \hat{S}_{ij}\hat{S}_{kl}$, $\hat{\mathbf{S}}^2 : \mathbf{D} = \hat{S}_{ij}\hat{S}_{kl}D_{kl}$ $\mathbf{N}\hat{\mathbf{S}} = N_{ij}\hat{S}_{kl}$, $\mathrm{tr}(\hat{\mathbf{S}}\mathbf{D}) = \hat{S}_{ij}D_{ij}$. The Euclidean standard of tensor $\mathbf{S}$ is $\|\mathbf{S}\| = \sqrt{S_{ij}S_{ij}}$.

The following extended constitutive relation applies to the hypoplastic model with intergranular strain:

$$\overset{\circ}{\mathbf{T}} = \mathcal{M}(\mathbf{T}, \mathbf{S}, e) : \mathbf{D} \qquad (B.1)$$

Owing to the third state variable, **S,** in which the previous directions of deformations accumulate, the model can no longer be represented by a single tensorial equation [8].

The normalised length of $\mathbf{S}$ is introduced for the 3D-formulation of the extended hypoplastic model:

$$\rho = \frac{\|\mathbf{S}\|}{R} \qquad (B.2)$$

where the material parameter R is the maximum intergranular strain. The direction of $\mathbf{S}$ is defined as follows:

$$\hat{\mathbf{S}} = \begin{cases} \mathbf{S}/\|\mathbf{S}\| & \text{for } \mathbf{S} \neq \mathbf{0} \\ \mathbf{0} & \text{for } \mathbf{S} = \mathbf{0} \end{cases} \qquad (B.3)$$

The equation required to develop the third state variable, $\mathbf{S}$, is dependent on the directions of the actual deformation, $\mathbf{D}$, and the intergranular strain, $\hat{\mathbf{S}}$, in relation to each other. This dependency is taken into account by the scalar product, $\mathrm{tr}(\hat{\mathbf{S}}\mathbf{D})$. The following relation applies in this case:

$$\overset{\circ}{\mathbf{S}} = \begin{cases} \mathbf{D} - \rho^{\beta_r}\cdot\hat{\mathbf{S}}^2 : \mathbf{D} & \text{for } \mathrm{tr}(\hat{\mathbf{S}}\mathbf{D}) > 0 \\ \mathbf{D} & \text{for } \mathrm{tr}(\hat{\mathbf{S}}\mathbf{D}) \leq 0 \end{cases} \qquad (B.4)$$

where $\overset{\circ}{\mathbf{S}}$ is the objective rate of intergranular strain [8]. The exponent β_r is a further material parameter.

Generally speaking, the following modified incremental stiffness

$$\mathcal{M} = \left[m_T\cdot\rho^{\chi} + m_R\cdot(1-\rho^{\chi})\right]\mathcal{L} + \begin{cases} (1-m_T)\cdot\rho^{\chi}\cdot\mathcal{L} : \hat{\mathbf{S}}^2 + \rho^{\chi}\cdot\mathbf{N}\hat{\mathbf{S}} & \text{for } \mathrm{tr}(\hat{\mathbf{S}}\mathbf{D}) > 0 \\ (m_R - m_T)\cdot\rho^{\chi}\cdot\mathcal{L} : \hat{\mathbf{S}}^2 & \text{for } \mathrm{tr}(\hat{\mathbf{S}}\mathbf{D}) \leq 0 \end{cases} \qquad (B.5)$$

is obtained from the hypoplastic tensorial functions $\mathcal{L}(\mathbf{T}, e)$ and $\mathbf{N}(\mathbf{T}, e)$ for any value of intergranular strain, i.e. $0 \leq \rho \leq 1$, and any directions of $\mathbf{D}$ and $\hat{\mathbf{S}}$. In eq. B.5, m_R, m_T and χ are the remaining three material parameters. The mode of operation of B.5 is, generally speaking, complex and is based on an interpolation of various extreme stiffness values [8].

In order to elucidate the characteristic stiffnesses, a distinction must first be made between $\rho = 1$, i.e. maximum intergranular strain, and $\rho = 0$, i.e. no intergranular strain.

In the first case, in which $\rho = 1$, there are three characteristic stiffnesses:

a) For continuous monotonic deformation with $\mathbf{D} \sim \hat{\mathbf{S}}$, eq. B.5 is simplified to:

$$\mathcal{M} = \mathcal{L} + \mathbf{N}\hat{\mathbf{S}}.$$

Eq. A.1 is obtained in this case as $\mathbf{N}\hat{\mathbf{S}} : \mathbf{D} = \mathbf{N}\|\mathbf{D}\|$, i.e. there is hypoplastic behaviour without intergranular strain.

b) For a deformation reversal, i.e. $\mathbf{D} \sim -\hat{\mathbf{S}}$, eq. B.5 is simplified to

$$\mathcal{M} = m_R\cdot\mathcal{L}.$$

As the second hypoplastic term $\mathbf{N}(\mathbf{T}, e)$ in eq. B.5 disappears in this case, there is hypoelastic behaviour with an increase in stiffness of $\mathcal{L}$, i.e. the material parameter m_R is greater than 1.

c) If there is a 90° change in the direction of the deformation rate, i.e. $\mathrm{tr}(\hat{\mathbf{S}}\mathbf{D}) = 0$, eq. B.5 is simplified to

$$\mathcal{M} = m_T\cdot\mathcal{L}.$$

There is hypoelastic behaviour as under b), but with a smaller increase in the stiffness of $\mathcal{L}$ than in b), i.e. the material parameter m_T is as follows: $m_R > m_T > 1$.

In the second case, in which $\rho = 0$, there is hypoelastic behaviour with increased stiffness, independent of the direction of **D**:

$$\mathcal{M} = m_R \cdot \mathcal{L} .$$

It should be noted that the reference state for a material with "pure" hypoplasticity is seen in case 1 a), but not in the second case.

The extended hypoplastic model with intergranular strain includes five additional material parameters:

- Maximum intergranular strain R [-],
- Increase factor at 180° change in direction m_R [-],
- Increase factor at 90° change in direction m_T [-],
- Exponent β_r [-],
- Exponent χ [-].

Annex C – Oedometric compression – Specification of L_{11} and N_1

Under the boundary conditions of uniaxial (oedometric) compression, the basic hypoplastic model is simplified by writing it as a matrix as follows:

$$\begin{Bmatrix} \Delta\sigma_1 \\ \Delta\sigma_2 \end{Bmatrix} = \begin{bmatrix} L_{11} & L_{12} \\ L_{21} & L_{22} \end{bmatrix} \begin{Bmatrix} \Delta\varepsilon_1 \\ 0 \end{Bmatrix} + \begin{Bmatrix} N_1 \\ N_2 \end{Bmatrix} |\Delta\varepsilon_1| \qquad (C.1)$$

The stress-strain relationship for oedometric compression can be computed by numerical integration with the aid of the upper row in (C.1). The components of $\mathcal{L}$ and **N** which it includes are as follows in accordance with (A.3) and (A.4):

$$L_{11} = f_s \frac{(1+2\cdot K)^2 + a^2}{1+2\cdot K^2} \qquad (C.2)$$

$$N_1 = f_s \cdot f_d \cdot \frac{a}{3} \cdot \frac{(1+2\cdot K)\cdot(5-2\cdot K)}{1+2\cdot K^2} \qquad (C.3)$$

The stress ratio $K = \sigma_2 / \sigma_1$ corresponds to the coefficient of the at rest value of earth pressure, K_0, in the case of monotonic loading.

References

[1] *Bauer, E.:* Zum mechanischen Verhalten granularer Stoffe unter vorwiegend ödometrischer Belastung. Veröff. Inst. für Bodenmech. u. Felsmech. der Universität Fridericiana in Karlsruhe, Heft 130, 1992.

[2] *Herle, I.:* Hypoplastizität und Granulometrie einfacher Korngerüste. Veröff. Inst. für Bodenmech. u. Felsmech. der Universität Frideri-ciana in Karlsruhe, Heft 142, 1997.

[3] *Herle, I., Gudehus, G.:* Determination of parameters of a hypoplastic constitutive model from properties of grain assemblies. Mechanics of Cohesive-frictional Materials, Vol. 4, 461-486, 1999.

[4] *Kayser, J., Schwab, R., Wachholz, T.:* Geotechnical aspects of constructing a new lock system next to an existing lock system. Proc ECSMFE, Amsterdam, Balkema, 1999.

[5] *Kolymbas, D.:* An outline of hypoplasticity. Archive of Applied Mechanics, Vol. 61, 43-151, 1991.

[6] *Kudella, P, Mayer, P.-M.:* Calculation of deformations using hypoplasticity demonstrated by the SONY-Center excavation in Berlin. Darmstadt Geotechnics, Darmstadt University of Technology. Ed. *R. Katzenbach* & *U. Arslan*, Vol. 1, 151-164, 1998.

[7] *Mayer, P-M.:* Verformungen und Spannungsänderungen durch Schlitzwandherstellung und Baugrubenaushub. Veröff. Inst. für Bodenmech. u. Felsmech. der Universität Fridericiana in Karlsruhe, Heft 151, 2000.

[8] *Mayer, P-M., Gudehus, G.:* Ermittlung von Bodenverschiebungen infolge Schlitzwandherstellung. Bautechnik 78, Nr. 7, 490-502, 2001.

[9] *Niemunis, A., Herle, I.:* Hypoplastic model for cohesionless soils with elastic strain range. Mechanics of Cohesive-frictional Materials, Vol. 2, 279-299, 1997.

[10] *Schwab, R., Kayser, J.:* An A-type prediction for a deep excavation near an existing navigable lock. Beyond 2000 in Computational Geotechnics. *Brinkgreve ed.*, Amsterdam, Balkema, 1999.

[11] *Wei Wu:* Hypoplastizität als mathematisches Modell zum mechanischen Verhalten granularer Stoffe. Veröff. Inst. für Bodenmech. u. Felsmech. der Universität Fridericiana in Karlsruhe, Heft 129, 1992.

[12] *von Wolffersdorff, P.-A.:* Verformungsprognosen für Stützkonstruktionen. Veröff. Inst. für Bodenmech. u. Felsmech. der Universität Fridericiana in Karlsruhe, Heft 141, 1997.

[13] *von Wolffersdorff, P.-A.:* A hypoplastic relation for granular materials with a predefined limit state surface. Mechanics of Cohesive-frictional Materials, Vol. 1, 251-271, 1996.

[14] *von Wolffersdorff, P.-A., Schwab, R.:* FE-Berechnungen für die Schleuse Uelzen unter Verwendung des hypoplastischen Stoffgesetzes. *Ohde* Kolloquium, Berlin, BAW, 1999.

Authors of the above article

Priv.-Doz. Dr.-Ing. habil. Peter-Andreas v. Wolffersdorff, Baugrund Dresden Ingenieurgesellschaft mbH, Paul-Schwarze-Strasse 2, 01097 Dresden

Dr.-Ing. Radu Schwab, Federal Waterways Engineering and Research Institute (BAW), Kussmaulstrasse 17, 76187 Karlsruhe